European Journal of Nuclear Medicine and Molecular Imaging (2019) 46:1531–1541
https://doi.org/10.1007/s00259-019-04320-9

ORIGINAL ARTICLE

Diagnostic performance of ^{68}Ga-PSMA PET/CT for identification of aggressive cribriform morphology in prostate cancer with whole-mount sections

Jie Gao[1] · Chengwei Zhang[1] · Qing Zhang[1] · Yao Fu[2] · Xiaozhi Zhao[1] · Mengxia Chen[1] · Bing Zhang[3] · Danyan Li[3] · Jiong Shi[2] · Feng Wang[4] · Hongqian Guo[1]

Received: 7 February 2019 / Accepted: 25 March 2019 / Published online: 25 April 2019

Abstract

Purpose To explore the diagnostic performance of ^{68}Ga-PSMA PET/CT for identification of pathological cribriform morphology in prostate cancer (PCa).

Methods The study retrospectively enrolled 49 PCa patients who had undergone preoperative multiparametric MRI (mpMRI) and ^{68}Ga-PSMA PET/CT, and who had Gleason pattern (GP) 4 and absence of GP 5 on radical prostatectomy specimens. Lesions with GP 4 were outlined and stratified according to their cribriform status. Volumes of interest were drawn on matched mpMRI and PET images, and parameters including average apparent diffusion coefficient (ADC_{mean}), tenth percentile ADC ($ADC_{10\%}$) and maximum standardized uptake value (SUV_{max}) were derived. The Mann-Whitney *U* test was used for continuous variables and the chi-squared test for categorical variables. Receiver operating characteristic analysis was used to compare imaging parameters in identifying cribriform morphology. The associations between cribriform-positive PCa and imaging variables were evaluated in a univariate analysis using a logistic regression model.

Results A total of 62 lesions were identified in 49 patients with GP 4. Of these lesions, 37 (59.7%) in 34 patients (69.4%) showed cribriform morphology. ADC_{mean} and $ADC_{10\%}$ were similar between cribriform-positive and non-cribriform groups ($P > 0.05$), while SUV_{max} was significantly different (median SUV_{max} 18.3 vs. 9.4 per patient, $P = 0.003$, 18.2 vs. 7.2 per lesion, $P < 0.001$), yielding sensitivities and specificities of 76% and 86% in a per-patient analysis, and 77% and 88% in a per-lesion analysis, respectively. Further, PSMA was significantly overexpressed in cribriform-positive PCa ($P = 0.003$). SUV_{max} was a significant predictor of cribriform morphology in PCa (odds ratio 8.61, 95% confidence interval 4.96–25.27, per patient; odds ratio 11.93, 95% confidence interval 6.49–33.74, per lesion; both $P < 0.001$).

Conclusion ^{68}Ga-PSMA PET/CT effectively identifies the aggressive cribriform morphology in PCa.

Keywords Prostate cancer · Multiparametric MRI · ^{68}Ga-PSMA PET/CT · Cribriform morphology

Jie Gao, Chengwei Zhang and Qing Zhang contributed equally to this work.

Electronic supplementary material The online version of this article (https://doi.org/10.1007/s00259-019-04320-9) contains supplementary material, which is available to authorized users.

✉ Feng Wang
fengwangcn@hotmail.com

✉ Hongqian Guo
dr.ghq@nju.edu.cn

[1] Department of Urology, Nanjing Drum Tower Hospital, The Affiliated Hospital of Nanjing University Medical School, Institute of Urology Nanjing University, No. 321 Zhongshan Road, Nanjing 210008, Jiangsu Province, China

[2] Department of Pathology, Nanjing Drum Tower Hospital, The Affiliated Hospital of Nanjing University Medical School, Nanjing, Jiangsu, China

[3] Department of Radiology, Nanjing Drum Tower Hospital, The Affiliated Hospital of Nanjing University Medical School, Nanjing, Jiangsu, China

[4] Department of Nuclear Medicine, Nanjing First Hospital, Nanjing Medical University, Nanjing, Jiangsu, China

Introduction

Prostate cancer (PCa), the most common cancer type and a major cause of cancer mortality in men in Europe and the United States, is a histologically heterogeneous and frequently multifocal disease [1, 2]. The Gleason scoring system, which scores the PCa pattern from 1 to 5 on the basis of the microscopic architecture, has guided the grading and risk stratification of PCa for over 50 years [3]. Cribriform morphology, a subtype of Gleason pattern (GP) 4, is recognized as a more aggressive and often more lethal architecture than non-cribriform morphologies of GP 4 (mainly fused and poorly formed architecture) [4, 5]. Over the past few years, many studies have demonstrated that cribriform-positive PCa is associated with an increased risk of lymph node invasion [6], distant metastasis [7], biochemical recurrence [8] and cancer-specific survival [9]. Hence, correct identification of the cribriform status of PCa is crucial for clinical decision-making.

Multiparametric magnetic resonance imaging (mpMRI) is currently regarded as the best imaging method to noninvasively identify and characterize PCa [10]. On the basis of level 1 evidence, mpMRI has recently been shown to improve the diagnosis of clinically significant PCa, and to help avoid unnecessary biopsies and the diagnosis of nonsignificant PCa [11, 12]. However, cribriform-predominant tumors are less visible [13], and in one study only 17% lesions of pure cribriform morphology were visible on MRI [14]. In a study comparing different biopsy techniques for the detection of cribriform morphology including MRI/ultrasonography fusion targeted biopsy, systematic biopsy and systematic plus targeted biopsy using radical prostatectomy (RP) as the reference standard, the combined approach demonstrated low sensitivity and specificity [14]. Promisingly, some parameters derived from apparent diffusion coefficient (ADC) maps such as average ADC (ADC_{mean}) and tenth percentile ADC ($ADC_{10\%}$), have been found to be significantly correlated with Gleason score (GS) [15, 16]. However, there was no significant difference in ADC_{mean}between cribriform-positive PCa and non-cribriform PCa [13, 17]. Due to the poor performance of mpMRI for identifying cribriform morphology, advanced imaging techniques are needed.

Positron emission tomography with prostate-specific membrane antigen ligands (e.g. ^{68}Ga-PSMA-11) is a relatively new nuclear imaging modality with highly promising performance for the detection of recurrent PCa [18–22], the diagnosis of primary PCa [23] and the evaluation of PCa aggressiveness [24, 25]. Indeed, increased pathological PSMA expression is correlated with tumor grade, pathological stage and biochemical recurrence [26], while tracer uptake on PSMA PET imaging is concordant with histologically determined PSMA expression [27]. Because of the usefulness of PSMA PET/CT for evaluating the aggressiveness of PCa, we hypothesized that PSMA PET/CT could be valuable for diagnosing aggressive cribriform morphology, an application that has not previously been studied.

In this study, we evaluated the ability of ^{68}Ga-PSMA PET/CT to distinguish cribriform-positive PCa from non-cribriform PCa in a consecutive cohort of men who had undergone surgical treatment.

Materials and methods

Patients

A total of 316 consecutive patients who had undergone RP between November 2017 and December 2018 were retrospectively identified. The inclusion criteria were as follows: (a) pathological diagnosis of prostate adenocarcinoma and availability of complete whole-mount step-section pathological slices; (b) preoperative 3.0 T mpMRI and ^{68}Ga-PSMA PET/CT within 3 months of surgery; (c) no neoadjuvant therapy before surgery; and (d) prostate cancer with GP 4 and absence of any GP 5 on final pathology. A flow chart of patient selection is shown in Fig. 1. Finally, a total of 49 patients were enrolled. Institutional review board approval was obtained and the study protocol was approved by the Ethics Committee of Nanjing Drum Tower Hospital (no. 2017-147-01), and all patients provided signed informed consent.

MRI examination

MpMRI examinations of the prostate were performed with a 3.0 T MR scanner (Achieva 3.0 T; Philips Medical Systems, The Netherlands) using a 32-channel phased-array coil. No endorectal coil was used. T2-weighted turbo spin-echo images (T2WI), diffusion-weighted spin-echo echo-planar images (DWI) with multiple *b* values (0/50/800/1,500 s/mm^2) and T1-weighted high-resolution isotropic volume with fat suppression after injection of 0.1 mmol/kg gadodiamide (GE Healthcare, Cork, Republic of Ireland) was used for dynamic contrast-enhanced imaging. Specific scanning parameters are shown in Supplementary Table 1. ADC maps were then generated from the DWI data on a Philips workstation using United Imaging software.

^{68}Ga-PSMA PET/CT examination

All patients were injected intravenously with ^{68}Ga-PSMA-11 (ABX Corporation, Radeberge, Germany) at a median dose 131.72 MBq (range 130.6–177.6 MBq). PET/CT was performed with a uMI 780 PET/CT scanner (United Imaging Healthcare, Shanghai, China). First, a CT scan (130 keV, 80 mAs, slice thickness 3.0 mm) was obtained 45 min after tracer

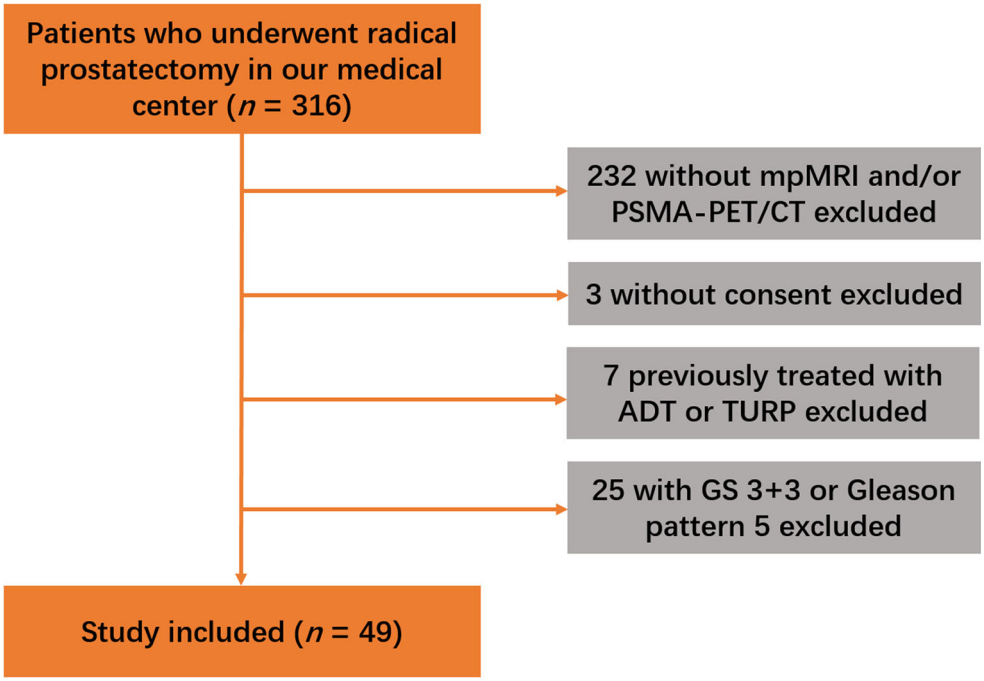

Fig. 1 Flow chart of patient selection (*ADT* androgen-deprivation therapy, *TURP* trans-urethral resection of the prostate, *GS* Gleason score)

injection without using contrast medium. Second, corrected for dead time, scatter and decay, static emission scans were acquired from the vertex to the proximal legs in three dimensions (matrix 200 × 200). This required eight bed positions with 3 min per bed position. The images were iteratively reconstructed and included CT-based attenuation correction using the OSEM algorithm with four iterations and eight subsets and gaussian filtering to an in-plane spatial resolution of 5 mm at full-width at half-maximum.

Whole-mount histopathology

After prostatectomy, prostate specimens were sliced from the apex to the base at 3-mm intervals. The slices were embedded in paraffin and stained with hematoxylin-eosin, and were then digitized at ×200 magnification using a whole-slide scanner (NanoZoomer S60; Hamamatsu, Japan). All digital slices were reviewed in consensus by two urological pathologists according to the 2014 International Society of Urological Pathology (ISUP) modified criteria for PCa [4]. Lesions with GP 4 were outlined and assigned a GS (3 + 4, 4 + 3 or 4 + 4). Major morphologies of GP 4 including fused, poorly formed and cribriform architecture were identified. Outlined regions were masked for further blinded radiopathological comparison.

MRI and PET/CT image evaluation

All MRI scans were reviewed in consensus by two radiologists. According to the Prostate Imaging Reporting and Data System v2 (PI-RADS v2), each lesion suspicious for PCa (PI-RADS score ≥3) was reported [10]. Then each case was reviewed to match each lesion outlined on the pathological slices with the corresponding mpMRI images by comparing the specific location, slide number and identifiable anatomic landmarks (such as urethra, ejaculatory ducts and benign prostatic hyperplasia). Histologically confirmed tumor corresponding to a previously identified lesion on mpMRI was considered visible. Subsequently, using MIStar software (Apollo Medical Imaging Technology, Australia), freehand regions of interest (ROI) were drawn on continuous axial ADC images following the outlines by pathologists. ADC_{mean} and $ADC_{10\%}$ were calculated from the histograms of pixel-wise ADC values within the whole-lesion volumes of interest (VOI) as previously described [15].

PET/CT images were evaluated in consensus by two nuclear medicine physicians including a double-trained board-certified physician. Similar to the procedure for MRI scans, suspicious lesions were reported and images were matched with the corresponding pathological slices. For each lesion, ROIs were drawn on continuous PET/CT fusion images using a RadiAnt DICOM viewer, 4.2.1 (Medixant, Poznan, Poland). The maximum standardized uptake values (SUV_{max}) were derived from the whole-lesion VOIs.

Immunohistochemistry

To compare the actual pathological PSMA expression between cribriform-positive PCa and non-cribriform PCa, two sets of ten patients were randomly selected from both groups. With available 3-μm formalin-fixed, paraffin-embedded whole-mount sections, Immunohistochemistry (IHC) was

done using monoclonal anti-PSMA (clone 1D6, 1:100, ZM-0476 from ZSGB-BIO) following the regular protocol provided by the manufacturer. As previously described [27, 28], the IHC results are reported as both percentage of positively stained cells and staining intensity, together with the immunoreactive score (IRS) and a modified four-point IRS classification (Supplementary Table 2). IHC analysis was performed by two independent investigators.

Statistical analysis

The Mann-Whitney *U* test was used for continuous variables and the chi-squared test for categorical variables. Receiver operating characteristic (ROC) analysis was used to compare the ability of imaging parameters to differentiate cribriform-positive PCa from non-cribriform PCa. The corresponding areas under the curve (AUC), cut-off values, and sensitivities and specificities for differentiation were calculated. The associations between cribriform-positive PCa and different preoperative variables were evaluated in a univariate analysis using a logistic regression model. Statistical analysis was performed using SPSS Statistics, version 21.0 (IBM Corp., Armonk, NY, USA). All tests were two-sided, with statistical significance set at $P < 0.05$.

Results

Patient characteristics and pathological classification

The demographic and clinical characteristics of the 49 patients are summarized in Table 1. The overall GS distribution of the index lesions was as follows: GS 3 + 4 in 19 of 49 (38.8%), GS 4 + 3 in 26 (53.1%), and GS 4 + 4 in 4 (8.1%). All separate foci of GP 4 were outlined on whole-mount sections, with an additional 12 foci of GS 3 + 4 and one focus of GS 4 + 3. In total, 62 lesions were identified. The distribution of specific morphological architectures is shown in Supplementary Table 3. Cribriform morphology was present in 34 of 49 patients (69.4%) and 37 of 62 lesions (59.7%).

Table 1 Characteristics of 49 patients

Characteristic	Value
Age (years), median (range)	69 (55–82)
Preoperative PSA (ng/ml), median (range)	15.94 (4.04–72.05)
Interval from MRI to RP (days), median (range)	22 (11–55)
Interval from PET/CT to RP (days), median (range)	11 (5–20)
Prostate volume (ml), median (range)	39 (17–107)
Index tumor diameter (cm), median (range)	1.9 (1.1–3.8)
Gleason score, *n* (%)	
3 + 4 = 7	19 (38.8)
4 + 3 = 7	26 (53.1)
4 + 4 = 8	4 (8.1)
pT stage, *n* (%)	
T2	12 (24.5)
T3a	28 (57.1)
T3b	9 (18.4)
T4	0 (0)
pN stage, *n* (%)	
N0	45 (91.8)
N1	4 (8.2)
Focality of lesion with Gleason pattern 4, *n* (%)	
One focus	38 (77.5)
Two foci	9 (18.4)
Three foci	2 (4.1)
Total number of lesions with Gleason pattern 4	62

PSA prostate-specific antigen, *RP* radical prostatectomy

Clinical and imaging characteristics stratified by cribriform status

Stratified by cribriform status, clinical and imaging characteristics were compared in both a per-patient and a per-lesion analysis. No significant differences were found in terms of patient age, preoperative PSA level, prostate volume, tumor diameter, pT stage and pN stage between cribriform-positive and non-cribriform PCa (Table 2). Regarding GS, cribriform morphology was more frequently present in GS 4 + 3 and 4 + 4 lesions than in 3 + 4 lesions in both the per-patient and per-lesion analysis ($P = 0.001$ and $P < 0.001$, respectively).

To further compare the imaging features, all lesions were matched on mpMRI, PET/CT and pathology. Representative radiopathological matching of non-cribriform and cribriform-positive lesions are shown in Fig. 2. One cribriform-positive index lesion, one non-cribriform index lesion and two non-cribriform non-index lesions were invisible on MRI ($P = 0.294$), while one cribriform-positive non-index lesion, one non-cribriform index lesion and four non-cribriform non-index lesions were invisible on PET ($P = 0.035$; Table 2). We also investigated the performance of PSMA PET imaging for primary staging (including extracapsular extension and seminal vesicle invasion) in the whole study population. The results are summarized in Supplementary Table 4. Generally, PSMA PET imaging demonstrated moderate sensitivity and considerable specificity in the diagnosis of both extracapsular extension and seminal vesicle invasion.

Parameters including PI-RADS score, ADC_{mean} and $ADC_{10\%}$ were similar in the two groups (all $P > 0.05$; Fig. 3, Table 2). Surprisingly, SUV_{max} was significantly higher in cribriform-positive PCa than in non-cribriform PCa in both the per-patient analysis (median 18.3 vs. 9.4, $P = 0.003$) and the per-lesion analysis (median 18.2 vs. 7.2, $P < 0.001$; Fig. 3, Table 2). There were also significant differences in SUV_{max} in

Table 2 Clinical and imaging characteristics stratified by cribriform status

Characteristic	Per-patient analysis[d]			Per-lesion analysis		
	Cribriform status		*P* value[e]	Cribriform status		*P* value[e]
	Yes	No		Yes	No	
No. of patients/lesions	34	15		37	25	
Age (years)	68 (65–74)	70 (62–75)	0.836	NA		
PSA (ng/ml)	14.6 (7.4–30.1)	14.1 (8.1–21.3)	0.678	NA		
Prostate volume (ml)	36 (27–41)	39 (35–74)	0.321	NA		
Tumor diameter (cm)	1.8 (1.4–2.5)	1.6 (1.3–2.5)	0.348	1.8 (1.3–2.5)	1.4 (0.8–2.0)	0.089
Gleason score, *n* (%)[a]						
3 + 4 = 7	8 (23.5)	11 (73.3)	**0.001**	11 (29.7)	20 (80.0)	**<0.001**
4 + 3 = 7	23 (67.6)	3 (20.0)		23 (62.2)	4 (16.0)	
4 + 4 = 8	3 (8.9)	1 (6.7)		3 (8.1)	1 (4.0)	
pT stage, *n* (%)[b]						
T2	7 (20.6)	5 (33.3)	0.473[f]	NA		
T3a	20 (58.8)	8 (53.3)				
T3b	7 (20.6)	2 (13.4)				
pN stage, *n* (%)						
N0	31 (91.2)	15 (100)	0.543[f]	NA		
N1	3 (8.8)	0 (0)				
Visible on MRI, *n* (%)	33 (97.0)	14 (93.3)	0.523[f]	36 (97.3)	22 (88.0)	0.294[f]
Visible on PET, *n* (%)	34 (100)	14 (93.3)	0.306[f]	36 (97.3)	20 (80.0)	**0.035[f]**
PI-RADS score, *n* (%)[c]						
3	0 (0)	0 (0)	0.321[c]	2 (5.7)	6 (27.3)	0.063
4	20 (60.6)	11 (78.6)		21 (60.0)	13 (54.6)	
5	13 (30.4)	3 (21.4)		13 (37.1)	3 (13.6)	
ADC_{mean} ($\mu m^2/s$)	649 (577–688)	598 (556–644)	0.115	645 (589–680)	630 (567–730)	0.687
$ADC_{10\%}$ ($\mu m^2/s$)	435 (349–514)	439 (365–513)	0.896	451 (354–507)	474 (368–571)	0.276
SUV_{max}	18.3 (10.6–25.9)	9.4 (7.7–10.3)	**0.003**	18.2 (11.1–25.5)	7.2 (5.1–9.8)	**<0.001**

Continuous variables are presented as medians (interquartile range)

PSA prostate specific antigen, *PI-RADS* Prostate Imaging Reporting and Data System, ADC_{mean} average ADC value, $ADC_{10\%}$ 10th percentile ADC value, SUV_{max} maximum standardized uptake value, *NA* not applicable

[a] Gleason score 3 + 4 vs. Gleason score 4 + 3/4 + 4

[b] pT2 vs. pT3

[c] PI-RADS 3/4 vs. PI-RADS 5, lesions visible on MRI were evaluated

[d] Parameters were derived from the index lesion on per-patient analysis

[e] *P* values <0.05 are indicated in bold

[f] Fisher's exact test

different GS and tumor diameter subgroups in relation to cribriform status (Supplementary Table 5).

Pathological PSMA expression stratified by cribriform status

We compared the actual pathological PSMA expression of non-cribriform PCa and cribriform-positive PCa. Representative cases are shown in Fig. 4a, b. In concordance with the imaging findings, 70% (7/10) of the non-cribriform PCa lesions showed an IRS of <4 (IRS classification 0 or 1), while 100% (10/10) of the cribriform-positive PCa lesions showed an IRS of ≥4 (IRS classification 2 or 3, $P = 0.003$; Fig. 4c, d).

Effectiveness of imaging parameters in differentiating cribriform status

Of the imaging parameters included in the PI-RADS score, ADC_{mean}, $ADC_{10\%}$ and SUV_{max}, SUV_{max} showed the highest

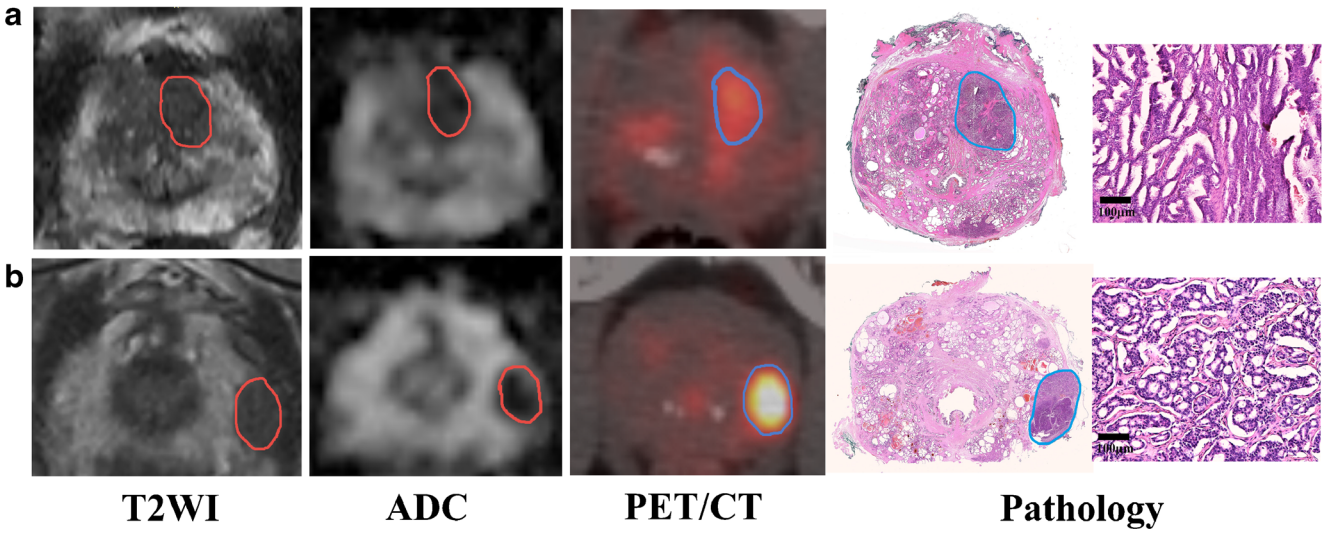

Fig. 2 Representative non-cribriform PCa lesions (**a**) and cribriform-positive PCa lesions (**b**). **a** A 69-year-old man with the index tumor in the transition zone (PSA level 8.05 ng/ml, GS 4 + 3, predominant fusion architecture of pattern 4, maximal diameter 1.5 cm), demonstrating a hypointense area on the T2-weighted and ADC images and moderate uptake on the PET/CT image. **b** A 73-year-old man with PCa in the transition zone (PSA level 17.76 ng/ml, GS 4 + 3, predominant cribriform architecture of pattern 4, maximal diameter 1.2 cm), demonstrating a hypointense area on the T2-weighted and ADC images and strong uptake on the PET/CT image. Lesions are outlined with solid lines on the MRI images, the PET/CT images and the pathological slices

AUC value of 0.80 (95% CI 0.68–0.91) in the per-patient analysis and 0.88 (95% CI 0.81–0.96) in the per-lesion analysis (Table 3). With a cut-off value of 10.9 for SUV_{max}, the sensitivities and specificities for cribriform status were 76% and 86% in the per-patient analysis, and 77% and 88% in the per-lesion analysis, respectively.

Univariate association between preoperative variables and cribriform-positive PCa

Using a logistic regression model, the univariate association between preoperative variables and cribriform-positive PCa were evaluated. Continuous variables including ADC_{mean},

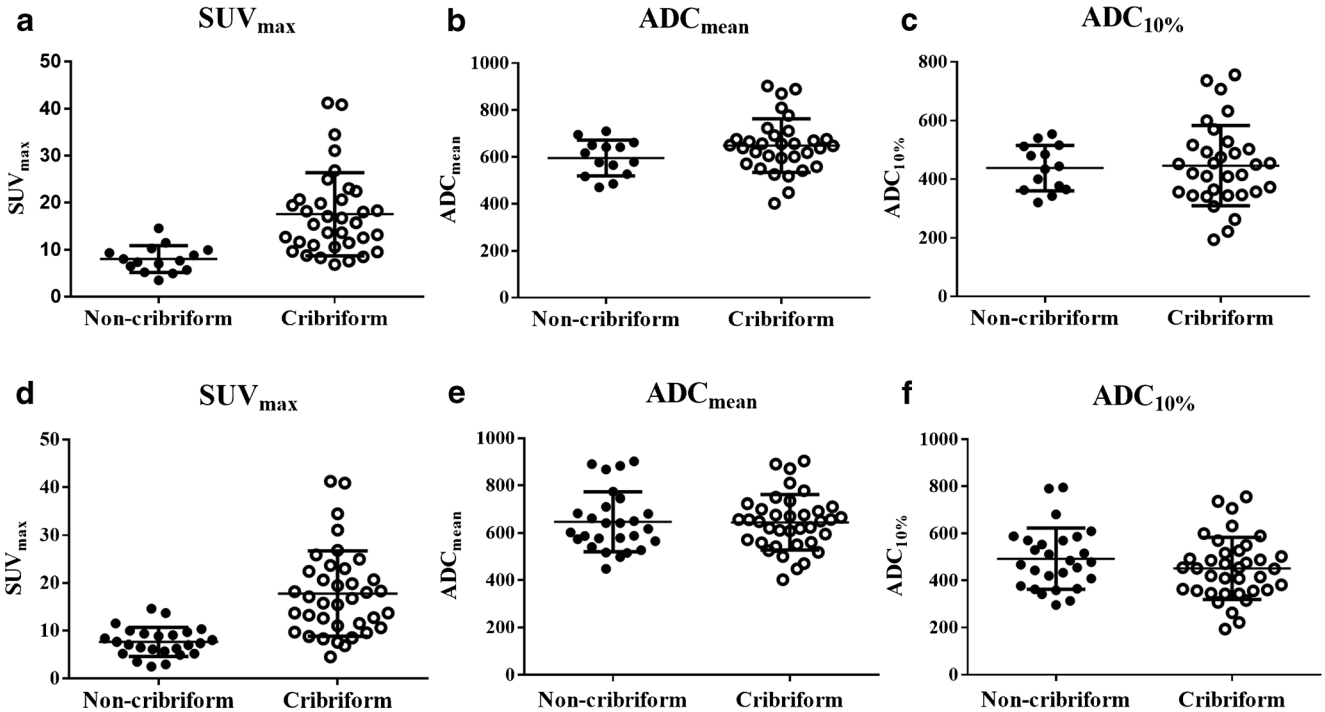

Fig. 3 Distribution of SUV_{max}, ADC_{mean} and $ADC_{10\%}$ in lesions in relation to cribriform status in the per-patient analysis (**a–c**) and the per-lesion analysis (**d–f**). *Solid lines* indicate means and standard deviations

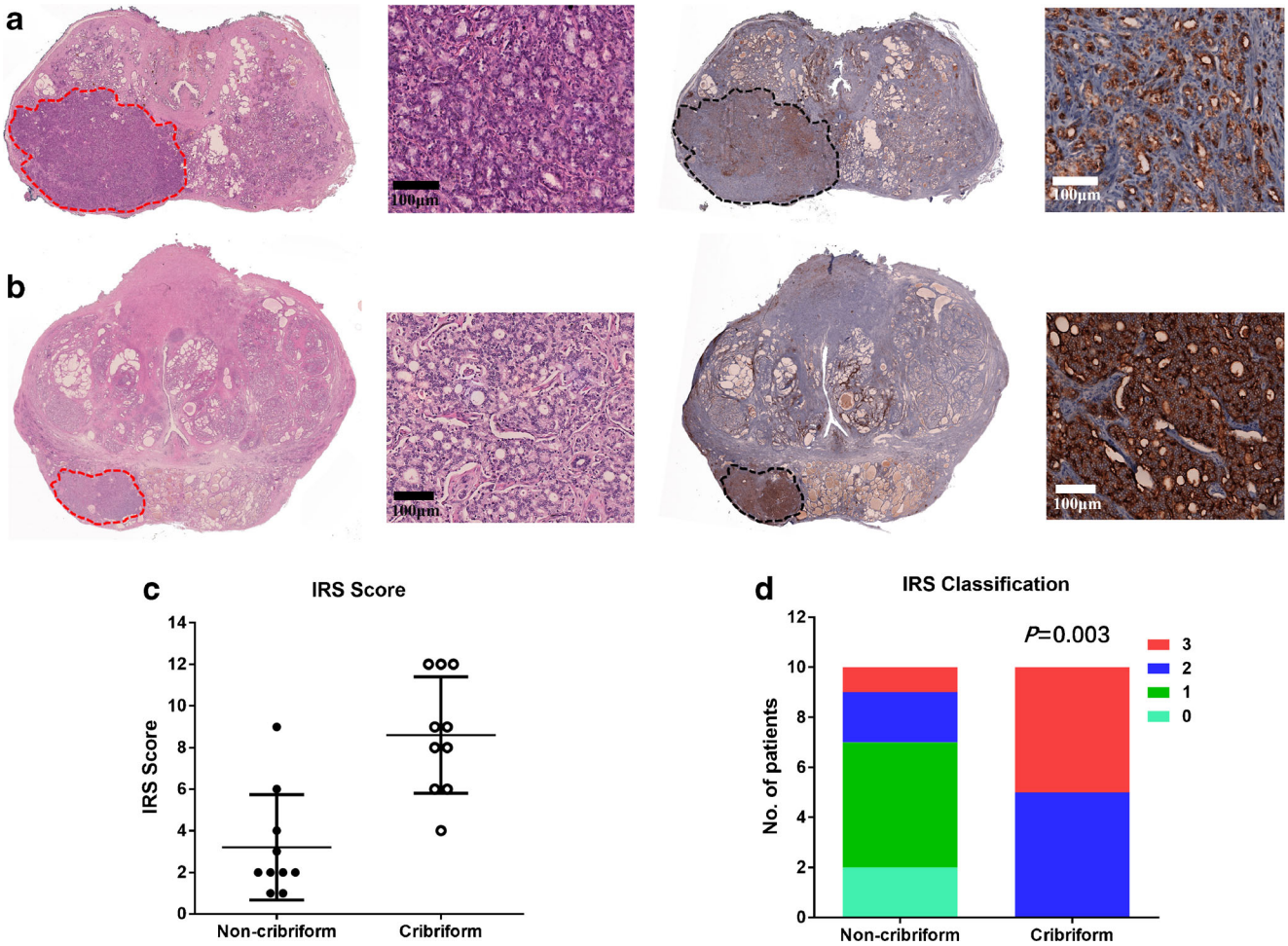

Fig. 4 Pathological PSMA expression in non-cribriform PCa ($n = 10$) and cribriform-positive PCa ($n = 10$) by immunohistochemistry. **a** A 55-year-old man with non-cribriform PCa (PSA level 17.31 ng/ml, GS 4 + 3, maximum diameter 2.2 cm), demonstrating primarily moderate staining for PSMA and IRS classification 2. **b** A 67-year-old man with cribriform-positive PCa (PSA level 5.46 ng/ml, GS 4 + 3, maximum diameter 1.1 cm), demonstrating strong staining for PSMA and IRS classification 3. **c**, **d** IRS score and IRS classification distribution according to cribriform status. **a**, **b** The *dashed lines* outline the lesions on both the pathological HE-stained slices and the IHC slices. **c** The *solid lines* indicate the means and standard deviations. **d** The *P* value was calculated using Fisher's exact test for IRS classification <2 vs. ≥2

$ADC_{10\%}$ and SUV_{max} were stratified by the cut-off values derived from the ROC analysis (Table 3). As shown in Table 4, a higher SUV_{max} was the only significant predictor of cribriform-positive PCa ($P < 0.001$), with odds ratios (OR) of 8.61 (95% CI 4.96–25.27) and 11.93 (95% CI 6.49–33.74) in the per-patient analysis and per-lesion analysis, respectively.

Discussion

To the best of our knowledge, this is the first study indicating the value of ^{68}Ga-PSMA PET/CT for identifying aggressive cribriform morphology in PCa. A higher SUV_{max} was a significant predictor of cribriform-positive PCa. Using the optimal cut-off value, the sensitivities and specificities for identifying cribriform status were 76% and 86% in the per-patient analysis, and 77% and 88% in the per-lesion analysis.

Cribriform morphology, which was described by Gleason as an architecture with "moderately differentiated glands, range from small to large, growing in spaced-out infiltrative patterns" [3], has received much attention recently. Dong et al. found that the presence of cribriform architecture was an independent predictor of biochemical recurrence as well as metastasis after RP [7]. In 2014, the ISUP conference reached a consensus that cribriform glands should be assigned a GP of 4, regardless of morphology [4]. Since the 2014 ISUP meeting, a rapidly growing body of evidence indicates the aggressive behavior of cribriform morphology as described above [5–9]. In our cohort, cribriform architecture was more frequently present in carcinoma with GS 4 + 3 or 4 + 4 and demonstrated larger tumor diameters than non-cribriform lesions, although the difference did not reach significance (Table 2).

Table 3 Effectiveness of imaging parameters in differentiating cribriform-positive PCa from non-cribriform PCa by ROC analysis

Variable	Per-patient analysis			Per-lesion analysis		
	AUC (95% CI)	Cut-off value	Sensitivity/specificity	AUC (95% CI)	Cut-off value	Sensitivity/specificity
PI-RADS score (3/4/5)	0.59 (0.42–0.76)	4	0.39/0.79	0.61 (0.47–0.76)	4	0.36/0.86
ADC_{mean} ($\mu m^2/s$)	0.65 (0.51–0.79)	618	0.65/0.53	0.62 (0.48–0.76)	618	0.71/0.57
$ADC_{10\%}$ ($\mu m^2/s$)	0.52 (0.37–0.67)	427	0.60/0.48	0.52 (0.38–0.65)	427	0.60/0.41
SUV_{max}	0.80 (0.68–0.91)	10.9	0.76/0.86	0.88 (0.81–0.96)	10.9	0.77/0.88

PI-RADS Prostate Imaging Reporting and Data System, *ADC_{mean}* average ADC value, *$ADC_{10\%}$* 10th percentile ADC value, *SUV_{max}* maximum standardized uptake value, *AUC* area under the curve, *CI* confidence interval

Regarding TNM stage, there were no significant associations between cribriform status and pT or pN stage. However, all three patients with positive lymph node extension had cribriform architecture (Table 2), which is a finding that warrants further attention.

MpMRI is currently regarded as the best imaging method to noninvasively identify and characterize PCa [10]. With PI-RADS v2, mpMRI demonstrated good performance for detecting PCa, with a pooled sensitivity of 89% and a specificity of 73% [29]. However, not all GP 4 morphologies were equivalently visible on MRI. The visibility of aggressive cribriform tumors was significantly lower than that of other GP 4 architectures across all ranges of tumor size [13], and only 17% lesions with pure cribriform morphology were visible on MRI [14]. Decreased visibility might theoretically be attributed to the relatively larger luminal perforations and fewer epithelial cells of cribriform morphology [13]. In this respect, aggressive cribriform morphology would be overlooked on MRI-guided targeted prostate biopsy. Indeed, several biopsy procedures including MRI-guided targeted biopsy have demonstrated poor sensitivity and specificity in the identification of cribriform morphology [14]. In our cohort, the percentages of lesions visible on MRI were similar between cribriform-positive and non-cribriform PCa (Table 2). Different stratification standards (predominant cribriform [13] or pure cribriform [14]) might explain the discrepant results. Moreover, parameters derived from ADC maps including ADC_{mean} and $ADC_{10\%}$ are applicable for PCa risk stratification [15, 16]. However, there were no significant differences in ADC_{mean} or $ADC_{10\%}$ between cribriform-positive and non-cribriform PCa in our cohort, in accordance with similar findings in previous studies [13, 17]. Considering the increasing use of mpMRI to identify candidates for active surveillance or focal therapy, mpMRI with advanced sequences or other alternative imaging techniques would be required to properly characterize aggressive cribriform morphology in PCa.

PSMA is a transmembrane protein with significantly increased expression in malignant PCa cells compared with that in normal prostate tissue, which is positively correlated with tumor grade, pathological stage and biochemical recurrence [26]. As a promising technique, ^{68}Ga-PSMA PET/CT imaging offers excellent performance in assessing primary tumor extent in PCa [23] and in detecting recurrent PCa [19–22]. Generally, PSMA PET imaging demonstrated moderate sensitivity and considerable specificity in diagnosing both extracapsular extension and seminal vesicle invasion in our cohort (Supplementary Table 4). Meanwhile, PSMA ligand uptake has already demonstrated good concordance with

Table 4 Univariate association between preoperative variables and cribriform-positive PCa

Variable	Per-patient analysis		Per-lesion analysis	
	OR (95% CI)	*P* value[a]	OR (95% CI)	*P* value[a]
Patient age	1.00 (0.92–1.10)	0.945	NA	
PSA level	1.03 (0.98–1.09)	0.197	NA	
Prostate volume	0.98 (0.96–1.01)	0.133	NA	
PI-RADS score (5 vs. 3/4)	2.38 (0.56–7.21)	0.242	3.74 (0.93–11.14)	0.064
ADC_{mean} ($\mu m^2/s$) (≥618 vs. <618)	2.86 (0.67–8.34)	0.158	2.09 (0.71–6.13)	0.179
$ADC_{10\%}$ ($\mu m^2/s$) (≥427 vs. <427)	0.67 (0.16–2.82)	0.582	0.56 (0.19–1.66)	0.298
SUV_{max} (≥10.9 vs. <10.9)	8.61 (4.96–25.27)	**<0.001**	11.93 (6.49–33.74)	**<0.001**

[a] *P* values <0.05 are indicated in bold

PSA prostate specific antigen, *PI-RADS* Prostate Imaging Reporting and Data System, *ADC_{mean}* average ADC value, *$ADC_{10\%}$* 10th percentile ADC value, *SUV_{max}* maximum standardized uptake value, *OR* odds ratio, *CI* confidence interval, *NA* not applicable

histopathological PSMA expression [27]. Taken together, PSMA PET imaging was able to noninvasively characterize the aggressiveness of PCa, which has been confirmed in several studies [24, 25]. In this study, we demonstrated the potential of PSMA PET imaging for the identification of cribriform morphology. Generally, 97.3% of cribriform-positive lesions were visible on PET, while 20% non-cribriform lesions were missed (Table 2). Surprisingly, SUV_{max}, a popular parameter derived from PET imaging, demonstrated excellent effectiveness in differentiating cribriform-positive PCa from non-cribriform PCa (Table 2, Fig. 3), yielding sensitivities and specificities of 76% and 86% in the per-patient analysis, and 77% and 88% in the per-lesion analysis, respectively (Table 3). Similar results were found in different GS and tumor diameter subgroups (Supplementary Table 5). We also found significant overexpression of PSMA in cribriform-positive PCa by IHC. The univariate analysis indicated that SUV_{max} was a significant predictor of cribriform-positive PCa (Table 4).

These results demonstrate that ^{68}Ga-PSMA PET/CT is applicable to the identification of cribriform morphology. In the clinical setting, in patients who have undergone preoperative PSMA PET imaging and who demonstrated a high SUV_{max} (more than 10.9), there would be high suspicion of the presence of cribriform morphology. In this situation, more biopsy cores to the suspicious target(s) could be taken for better detection of cribriform morphology. Furthermore, cribriform risk obtained from PET imaging helps with the decision on ruling out candidates for active surveillance or focal therapy. Additionally, patients with the suspicion of cribriform-positive PCa should receive more radical surgical treatment than those with non-cribriform PCa.

Recently, integrated PET/MRI, which combines the strengths of both modalities, has been shown to have great potential for influencing clinical practice by providing a more certain map of localized PCa to aid targeted biopsies and therapy, and to improve the detection of biochemical recurrence and the staging of metastatic disease [30–32]. Because of the potential of PET to image cribriform morphology, it is expected that PET/MRI could also be used to detect cribriform morphology.

Of course, our study had some limitations. First, the data were retrospectively collected, and we used final RP pathology as the reference standard. Hence, a selection bias might have occurred. Nonetheless, the final RP specimen, especially in the form of whole-mount sections, is the most accurate determinant of the presence or absence of cribriform morphology. Second, according to the study aim, we enrolled only patients/lesions with a GP of 4, which might restrict clinical application to the general population. However, given that the SUV_{max} of GS 8–10 PCa was significantly higher than that of GS 6–7 PCa found in several studies [20, 21], we believed that with the cut-off value, aggressive phenotypes including cribriform-positive PCa and GS 8–10 PCa could effectively be selected. Third, our sample size was relatively small although, to compensate, we included every lesion on all images. Fourth, considering the relatively high OR of SUV_{max} and the relatively small study group, we did not perform a multivariate analysis. Further research with a larger sample size is necessary for confirmation.

Conclusion

Our study indicates that ^{68}Ga-PSMA PET/CT could effectively identify aggressive cribriform morphology in PCa. These results may help with the decision on ruling out candidates for active surveillance or focal therapy. Additionally, patients with suspicion of cribriform-positive PCa should receive more radical treatment than those with non-cribriform PCa.

Funding This research was supported by the National Natural Science Foundation of China (ID 81772710, 81572519, 81802535 and 81602221), the Project of Invigorating Health Care through Science, Technology and Education, Jiangsu Provincial Key Medical Discipline (Laboratory) (ZDXKB2016014) and the National Natural Science Foundation of Jiangsu Province (BK20160117).

Compliance with ethical standards

Conflicts of interest None.

Ethical approval All procedures performed in studies involving human participants were in accordance with the ethical standards of the institutional and/or national research committee and with the principles of the 1964 Declaration of Helsinki and its later amendments or comparable ethical standards.

Informed consent Informed consent was obtained from all individual participants included in the study.

Abbreviations *ADC*, Apparent diffusion coefficient; ADC_{mean}, Average apparent diffusion coefficient; $ADC_{10\%}$, Tenth percentile apparent diffusion coefficient; *AUC*, Area under the curve; *DWI*, Diffusion-weighted imaging; *GP*, Gleason pattern; *GS*, Gleason score; *IHC*, Immunohistochemistry; *IRS*, Immunoreactive score; *mpMRI*, Multiparametric magnetic resonance imaging; *PCa*, Prostate cancer; *PET/CT*, Positron emission tomography/computed tomography; *PI-RADS*, Prostate Imaging Reporting and Data System; *PSA*, Prostate-specific antigen; *PSMA*, Prostate-specific membrane antigen; *RP*, Radical prostatectomy; *ROC*, Receiver operating characteristic; SUV_{max}, Maximum standardized uptake value

References

1. Siegel RL, Miller KD, Jemal A. Cancer statistics, 2017. CA Cancer J Clin. 2017;67:7–30. https://doi.org/10.3322/caac.21387.
2. Le JD, Tan N, Shkolyar E, Lu DY, Kwan L, Marks LS, et al. Multifocality and prostate cancer detection by multiparametric magnetic resonance imaging: correlation with whole-mount

histopathology. Eur Urol. 2015;67:569–76. https://doi.org/10.1016/j.eururo.2014.08.079.
3. Gleason DF. Classification of prostatic carcinomas. Cancer Chemother Rep. 1966;50:125–8.
4. Epstein JI, Egevad L, Amin MB, Delahunt B, Srigley JR, Humphrey PA. The 2014 International Society of Urological Pathology (ISUP) consensus conference on Gleason grading of prostatic carcinoma: definition of grading patterns and proposal for a new grading system. Am J Surg Pathol. 2016;40:244–52. https://doi.org/10.1097/pas.0000000000000530.
5. Truong M, Frye T, Messing E, Miyamoto H. Historical and contemporary perspectives on cribriform morphology in prostate cancer. Nat Rev Urol. 2018;15:475–82. https://doi.org/10.1038/s41585-018-0013-1.
6. Kryvenko ON, Gupta NS, Virani N, Schultz D, Gomez J, Amin A, et al. Gleason score 7 adenocarcinoma of the prostate with lymph node metastases: analysis of 184 radical prostatectomy specimens. Arch Pathol Lab Med. 2013;137:610–7. https://doi.org/10.5858/arpa.2012-0128-OA.
7. Dong F, Yang P, Wang C, Wu S, Xiao Y, McDougal WS, et al. Architectural heterogeneity and cribriform pattern predict adverse clinical outcome for Gleason grade 4 prostatic adenocarcinoma. Am J Surg Pathol. 2013;37:1855–61. https://doi.org/10.1097/PAS.0b013e3182a02169.
8. Kir G, Sarbay BC, Gumus E, Topal CS. The association of the cribriform pattern with outcome for prostatic adenocarcinomas. Pathol Res Pract. 2014;210:640–4. https://doi.org/10.1016/j.prp.2014.06.002.
9. Harding-Jackson N, Kryvenko ON, Whittington EE, Eastwood DC, Tjionas GA, Jorda M, et al. Outcome of Gleason 3 + 5 = 8 prostate cancer diagnosed on needle biopsy: prognostic comparison with Gleason 4 + 4 = 8. J Urol. 2016;196:1076–81. https://doi.org/10.1016/j.juro.2016.05.105.
10. Weinreb JC, Barentsz JO, Choyke PL, Cornud F, Haider MA, Macura KJ, et al. PI-RADS prostate imaging – reporting and data system: 2015, version 2. Eur Urol. 2016;69:16–40. https://doi.org/10.1016/j.eururo.2015.08.052.
11. Ahmed HU, El-Shater Bosaily A, Brown LC, Gabe R, Kaplan R, Parmar MK, et al. Diagnostic accuracy of multi-parametric MRI and TRUS biopsy in prostate cancer (PROMIS): a paired validating confirmatory study. Lancet. 2017;389:815–22. https://doi.org/10.1016/s0140-6736(16)32401-1.
12. Kasivisvanathan V, Rannikko AS, Borghi M, Panebianco V, Mynderse LA, Vaarala MH, et al. MRI-targeted or standard biopsy for prostate-cancer diagnosis. N Engl J Med. 2018;378:1767–77. https://doi.org/10.1056/NEJMoa1801993.
13. Truong M, Hollenberg G, Weinberg E, Messing EM, Miyamoto H, Frye TP. Impact of Gleason subtype on prostate cancer detection using multiparametric magnetic resonance imaging: correlation with final histopathology. J Urol. 2017;198:316–21. https://doi.org/10.1016/j.juro.2017.01.077.
14. Truong M, Feng C, Hollenberg G, Weinberg E, Messing EM, Miyamoto H, et al. A comprehensive analysis of cribriform morphology on magnetic resonance imaging/ultrasound fusion biopsy correlated with radical prostatectomy specimens. J Urol. 2018;199:106–13. https://doi.org/10.1016/j.juro.2017.07.037.
15. Donati OF, Mazaheri Y, Afaq A, Vargas HA, Zheng J, Moskowitz CS, et al. Prostate cancer aggressiveness: assessment with whole-lesion histogram analysis of the apparent diffusion coefficient. Radiology. 2014;271:143–52. https://doi.org/10.1148/radiol.13130973.
16. Peng Y, Jiang Y, Antic T, Giger ML, Eggener SE, Oto A. Validation of quantitative analysis of multiparametric prostate MR images for prostate cancer detection and aggressiveness assessment: a cross-imager study. Radiology. 2014;271:461–71. https://doi.org/10.1148/radiol.14131320.
17. Hurrell SL, McGarry SD, Kaczmarowski A, Iczkowski KA, Jacobsohn K, Hohenwalter MD, et al. Optimized b-value selection for the discrimination of prostate cancer grades, including the cribriform pattern, using diffusion weighted imaging. J Med Imaging. 2018;5:011004. https://doi.org/10.1117/1.jmi.5.1.011004.
18. Perera M, Papa N, Christidis D, Wetherell D, Hofman MS, Murphy DG, et al. Sensitivity, specificity, and predictors of positive (68)Ga-prostate-specific membrane antigen positron emission tomography in advanced prostate cancer: a systematic review and meta-analysis. Eur Urol. 2016;70:926–37. https://doi.org/10.1016/j.eururo.2016.06.021.
19. Afshar-Oromieh A, Holland-Letz T, Giesel FL, Kratochwil C, Mier W, Haufe S, et al. Diagnostic performance of (68)Ga-PSMA-11 (HBED-CC) PET/CT in patients with recurrent prostate cancer: evaluation in 1007 patients. Eur J Nucl Med Mol Imaging. 2017;44:1258–68. https://doi.org/10.1007/s00259-017-3711-7.
20. Caroli P, Sandler I, Matteucci F, De Giorgi U, Uccelli L, Celli M, et al. (68)Ga-PSMA PET/CT in patients with recurrent prostate cancer after radical treatment: prospective results in 314 patients. Eur J Nucl Med Mol Imaging. 2018;45:2035–44. https://doi.org/10.1007/s00259-018-4067-3.
21. Zacho HD, Nielsen JB, Afshar-Oromieh A, Haberkorn U, deSouza N, De Paepe K, et al. Prospective comparison of (68)Ga-PSMA PET/CT, (18)F-sodium fluoride PET/CT and diffusion weighted-MRI at for the detection of bone metastases in biochemically recurrent prostate cancer. Eur J Nucl Med Mol Imaging. 2018;45:1884–97. https://doi.org/10.1007/s00259-018-4058-4.
22. Ceci F, Castellucci P, Graziani T, Farolfi A, Fonti C, Lodi F, et al. (68)Ga-PSMA-11 PET/CT in recurrent prostate cancer: efficacy in different clinical stages of PSA failure after radical therapy. Eur J Nucl Med Mol Imaging. 2019;46:31–9. https://doi.org/10.1007/s00259-018-4189-7.
23. Sachpekidis C, Kopka K, Eder M, Hadaschik BA, Freitag MT, Pan L, et al. 68Ga-PSMA-11 dynamic PET/CT imaging in primary prostate cancer. Clin Nucl Med. 2016;41:e473–9. https://doi.org/10.1097/rlu.0000000000001349.
24. Koerber SA, Utzinger MT, Kratochwil C, Kesch C, Haefner MF, Katayama S, et al. (68)Ga-PSMA-11 PET/CT in newly diagnosed carcinoma of the prostate: correlation of Intraprostatic PSMA uptake with several clinical parameters. J Nucl Med. 2017;58:1943–8. https://doi.org/10.2967/jnumed.117.190314.
25. Uprimny C, Kroiss AS, Decristoforo C, Fritz J, von Guggenberg E, Kendler D, et al. (68)Ga-PSMA-11 PET/CT in primary staging of prostate cancer: PSA and Gleason score predict the intensity of tracer accumulation in the primary tumour. Eur J Nucl Med Mol Imaging. 2017;44:941–9. https://doi.org/10.1007/s00259-017-3631-6.
26. Ross JS, Sheehan CE, Fisher HA, Kaufman RP Jr, Kaur P, Gray K, et al. Correlation of primary tumor prostate-specific membrane antigen expression with disease recurrence in prostate cancer. Clin Cancer Res. 2003;9:6357–62.
27. Woythal N, Arsenic R, Kempkensteffen C, Miller K, Janssen JC, Huang K, et al. Immunohistochemical validation of PSMA expression measured by (68)Ga-PSMA PET/CT in primary prostate cancer. J Nucl Med. 2018;59:238–43. https://doi.org/10.2967/jnumed.117.195172.
28. Kaemmerer D, Peter L, Lupp A, Schulz S, Sanger J, Prasad V, et al. Molecular imaging with (68)Ga-SSTR PET/CT and correlation to immunohistochemistry of somatostatin receptors in neuroendocrine tumours. Eur J Nucl Med Mol Imaging. 2011;38:1659–68. https://doi.org/10.1007/s00259-011-1846-5.
29. Woo S, Suh CH, Kim SY, Cho JY, Kim SH. Diagnostic performance of Prostate Imaging Reporting and Data System version 2 for detection of prostate cancer: a systematic review and diagnostic meta-analysis. Eur Urol. 2017;72:177–88.

30. Eiber M, Weirich G, Holzapfel K, Souvatzoglou M, Haller B, Rauscher I, et al. Simultaneous (68)Ga-PSMA HBED-CC PET/MRI improves the localization of primary prostate cancer. Eur Urol. 2016;70:829–36. https://doi.org/10.1016/j.eururo.2015.12.053.

31. Kranzbuhler B, Nagel H, Becker AS, Muller J, Huellner M, Stolzmann P, et al. Clinical performance of (68)Ga-PSMA-11 PET/MRI for the detection of recurrent prostate cancer following radical prostatectomy. Eur J Nucl Med Mol Imaging. 2018;45:20–30. https://doi.org/10.1007/s00259-017-3850-x.

32. Hicks RM, Simko JP, Westphalen AC, Nguyen HG, Greene KL, Zhang L, et al. Diagnostic accuracy of (68)Ga-PSMA-11 PET/MRI compared with multiparametric MRI in the detection of prostate cancer. Radiology. 2018;289:730–7. https://doi.org/10.1148/radiol.2018180788.